Environmental Fluid Mechanics
https://doi.org/10.1007/s10652-019-09696-8

ORIGINAL ARTICLE

Plumes in a rotating two-layer stratified fluid

Yongxing Ma[1] · **Morris R. Flynn**[2] · **Bruce R. Sutherland**[3]

Received: 16 November 2018 / Accepted: 3 June 2019

Abstract
Laboratory experiments are conducted to examine a descending plume in a rotating two-layer stratified ambient fluid such that the plume at the interface has moderate to large Rossby number. While the source fluid is more dense than the lower layer, the experiments are designed so that the mean density of the plume fluid impinging upon the interface is less than the lower layer density, as represented by a buoyancy parameter, Λ, being less than unity. In such cases, the discharged plume fluid spreads radially at the interface in the form of an intrusive gravity current at early times. At later times, this intrusion evolves to form an anticyclonic lens due to the influence of the Coriolis force. The measured radial position of the intrusion front, $R(t)$, follows different power law relationships at early and late times during the spread of the intrusion: at early times when rotation does not play a significant role the power law exponent lies between 0.5 and 1.1; at late times when the intrusion acts as a rotationally influenced expanding lens the power law exponent ranges between 0.15 and 0.5, with generally smaller values for larger Λ. The plume fluid reaching the interface progressively increases in density due to re-entraining relatively dense fluid as the plume descends within the thickening lens. Consequently, the plume eventually penetrates through the interface and descends to the bottom of the tank. Faster rotation makes the lens thicker and hence increases the volume of the re-entrained lens-fluid, which decreases the time for the onset of penetration. The penetration time normalized by the rotation rate is found to hold a simple power law relationship with Λ.

Keywords Plumes · Stratification · Rotation · Interfacial gravity current · Geostrophic spreading

✉ Bruce R. Sutherland
bruce.sutherland@ualberta.ca

[1] Department Earth and Atmospheric Sciences, University of Alberta, Edmonton, AB T6G 2E3, Canada

[2] Department of Mechanical Engineering, University of Alberta, Edmonton, AB T6G 1H9, Canada

[3] Departments of Physics and of Earth and Atmospheric Sciences, University of Alberta, Edmonton, AB T6G 2E1, Canada

Published online: 10 June 2019

1 Introduction

Turbulent plumes have been well investigated since the seminal study of Morton et al. [21], referred to hereafter as MTT, who developed an integral model for a plume in a non-rotating semi-infinite domain. This model was adapted by Baines and Turner [3] to account for the evolution of a plume in an ambient fluid of finite size. As the plume reached the opposite (horizontal) boundary, being a solid surface in the case of a descending plume or a solid surface or free surface in the case of an ascending plume, discharged plume fluid spread horizontally to the vertical walls of the control volume and then a stratified layer formed. This stratified layer progressively thickened as a result of the continual discharge of plume fluid. The plume itself was modified through entrainment of the ambient fluid, whose density changed as a continuous function of time.

More recently the evolution of plumes in a two-layer ambient fluid have been studied through laboratory experiments [18, 22]. In order to classify whether the plume is capable of penetrating through the density interface of the ambient fluid, a buoyancy parameter, Λ, was introduced by Mott and Woods [22] as a measure of the mean density of the plume fluid at the interface compared with the lower layer density. When $\Lambda < 1$, meaning the plume at the interface is initially lighter than the lower layer, the plume fluid spreads horizontally at the interface. Kumagai [18] and Mott and Woods [22] regarded the density interface of the ambient fluid as a false bottom for a filling-box process that was restricted to the upper layer. Due to partial re-entrainment of the intrusion into the plume and entrainment into the fountain-head (usually referred to as "fountain-top" for an ascending plume), the plume eventually penetrated through the interface when its density at the interface exceeded the density, ρ_l, of the lower layer. In both of [18] and [22], the penetration onset time (or, more simply, the penetration time) was found to depend on Λ and the horizontal cross-sectional area of the tanks in their (non-rotating) experiments.

Here we extend these studies to examine the influence of the Coriolis force on plume spreading and ultimate penetration through a density interface. There are few studies of plumes in a rotating stratified environment. This gap in the literature is somewhat surprising because any plume that evolves over long times and in sufficiently large domains must eventually become influenced by both the Coriolis force and stratification. Examples include giant volcanic eruptions [2], vertical convection under polynyas [23] and under-sea oil blow-outs [12].

In experiments with $\Lambda < 1$, the plume is expected to spread radially at the interface as in Kumagai [18] and Mott and Woods [22]. However, in the presence of rotation Coriolis forces retard the lateral spread of the discharged plume fluid along the density interface of the ambient fluid as the spreading fluid forms an anticyclonic lens. With lateral boundaries playing a comparatively insignificant role vs. the non-rotating case, the dynamics of rotation acting upon the spreading fluid is crucial to setting the eventual time for penetration of plume fluid through the density interface of the ambient fluid. These dynamics are explored here.

If the density interface is not too far below the plume source so that the plume's associated Rossby number is sufficiently larger than unity when it reaches the interface, then the influence of the background rotation on the plume and the interfacial intrusion that first spreads radially from the plume is insignificant at early times. Thus the interfacial intrusion can be treated as an intrusive gravity current in non-rotating environment. For non-rotating constant-flux axisymmetric intrusions at a solid boundary, the radius is predicted to increase with time as a 3 / 4 power law [4]. One might expect a similar power law for

the initial spreading of a plume at a solid bottom boundary over sufficiently early times that rotation effects are not yet significant. However, for a plume spreading at an interface, the effects of fountain-head entrainment of lower layer fluid into the rebounding plume may alter this law through its influence on the buoyancy flux. Likewise, in a two-layer stratified ambient fluid, the ratio of the upper to lower layer densities will dictate the fraction of the intrusion that propagates above vs. below the interface. Taking these factors into account, but ignoring the relatively minor influence of internal or inertial waves, which are estimated from numerical studies to convert only 3–5% of the energy associated with the incident plume [8, 9], the relationship between the radius of the intrusion and time will be affected by the lower layer fluid density. This circumstance has not been thoroughly examined in the literature. Better studied is the case of a plume spreading at its neutral buoyancy level in uniform stratification for which one predicts the radius to increase in time, t, as a 2 / 3 power law if entrainment into the intrusion is neglected (the volume flux is constant) [19, 24, 26] or as a 3/4 power law if the buoyancy flux is constant [24]. Separate laboratory investigations have been performed to assess the vertical growth of the fluid discharged by a plume in a uniformly stratified ambient. Thus did Whitehead et al. [29] and Colomer et al. [7] respectively argue that the initial maximum depth of the convective mixed layer located beneath the plume source ought to scale as $t^{1/2}$ and t^{1}.

Coriolis forces eventually act to deflect the radially expanding fluid such that the intrusion then grows radially and in thickness as an anticyclonic lens. As a special case, Griffiths and Linden [13] discharged light fluid upon the free surface of a dense ambient fluid in solid-body rotation. They found that if the source volume flux was sufficiently small, the spreading fluid formed an anticyclonic lens that gradually expanded in a quasi-steady state dictated by a cyclogeostrophic balance of buoyancy, Coriolis and centrifugal forces. In particular, they predicted that the radius should increase in time as a 1 / 4 power law. Building on Griffiths and Linden's study, Helfrich and Battisti [14] examined the spread at its neutral buoyancy level of a plume in a rotating uniformly stratified fluid. They assumed the lens formed a self-similar shape such that the aspect ratio of lens height to radius remained constant [5, 14]. Additionally assuming a constant volume flux into the lens, the radius is expected to increase as a 1/3 power of time [30]. However, these previous studies differ in important ways from the scenario of a plume spreading along a sharp density interface. In this latter case the density of plume-fluid entering the lens increases in time as the lens thickness increases and the top of the lens approaches the plume source uninhibited by ambient stratification; the plume acquires, through the process of entrainment, cyclonic vorticity before entering the lens; and once inside the lens, the plume entrains lens fluid, which is then later detrained toward the lower part of the lens. As a result of these factors, we expect a complicated vertical structure of radial flow and density stratification within the lens.

The background rotation also acts on the free surface and density interface of the two-layer stratified ambient fluid. In solid body rotation the centrifugal force is balanced by the pressure gradient resulting from the parabolic deflection of the free surface and the density interface. The interface between the upper and lower layers has the same parabolic shape as the free surface regardless of the density jump across the density interface of the ambient fluid [27]. For the experiments reported upon here, the maximum slope of the deflected interface is less than 0.01. Thus, although the advance of the interfacial intrusion ostensibly could be influenced by the conversion of kinetic to potential energy as it runs upslope, this effect is expected to be insignificant.

Even neglecting the influence of the deflected free surface and stratification, plumes are eventually impacted by background rotation. In studies of point source plumes in a uniform

density ambient fluid, Fernando et al. [10] showed experimentally that the speed of descent of the plume front decreased for $t > 2.4/\Omega$, where Ω is the background rotation rate. They attributed this deceleration to the alteration by the Coriolis force of the horizontal inflow associated with plume entrainment. This horizontal flow in the ambient fluid developed into a cyclonic circulation that retarded inflow and entrainment into the plume. As a consequence, and consistent with analogue laboratory experiments of line source plumes [11] and (turbulent) thermals [1] falling through a rotating environment, the radius of the point source plume became effectively constant at some critical vertical distance from the source corresponding to the Rossby number of the plume becoming close to unity. In turn, the circulation of ambient fluid around the plume eventually triggered baroclinic instability. As found by Tomas et al. [28] in numerical simulations and by Frank et al. [12] in laboratory experiments, background rotation may also induce an anticyclonic precession of the plume near the source. The frequency of precession, ω, was measured by Frank et al. [12] to be proportional to the angular frequency of rotation, Ω, such that $\omega \approx (0.40 \pm 0.04)\Omega$.

In light of the above considerations, models of the spreading rate and spreading height of a lens formed from the fluid discharged by a plume impinging on a density interface in the presence of background rotation remain inconclusive with several outstanding theoretical challenges. It is beyond the scope of this paper to develop such a theory. Rather, and seeking to inform theoretical model development, we report upon the results of laboratory experiments that demonstrate a collapse of data when the non-dimensional plume penetration time is plotted against Λ. Likewise we consider the dependence upon Λ of the radial spread of the intrusion at early times and of the expanding rotationally-influenced lens at late times before penetration occurs.

The rest of the manuscript is organized as follows. In Sect. 2, previous theories describing plumes in a non-rotating ambient fluid and intrusions in a non-rotating and rotating ambient fluid are summarized and adapted to the present experiments. The set up of the experiments are described in Sect. 3 and the experiment analysis methods and results are presented in Sect. 4. Discussion and conclusions are given in Sect. 5.

2 Theory

In our study, a downward-propagating plume originates near the free surface and descends to the density interface of a rotating two-layer ambient fluid, as illustrated in Fig. 1. Of interest is the circumstance in which the plume is less dense than the lower layer ambient fluid when it first reaches the interface so that it then spreads as an intrusive gravity current. Later, the Coriolis force impedes the radial advance of this intrusion and it evolves into a quasi-geostrophically balanced lens until potentially becoming more dense than the lower layer and so descending to depth. From the above physical description, we present below a series of equations meant to give preliminary guidance in the interpretation of select experimental results, laboratory measurements being the focal point of our research. As noted above, we defer to future work the more involved task of devising from first principles a comprehensive theory that accounts for all of the complications of the plume and lens evolution as they are influenced by stratification and rotation.

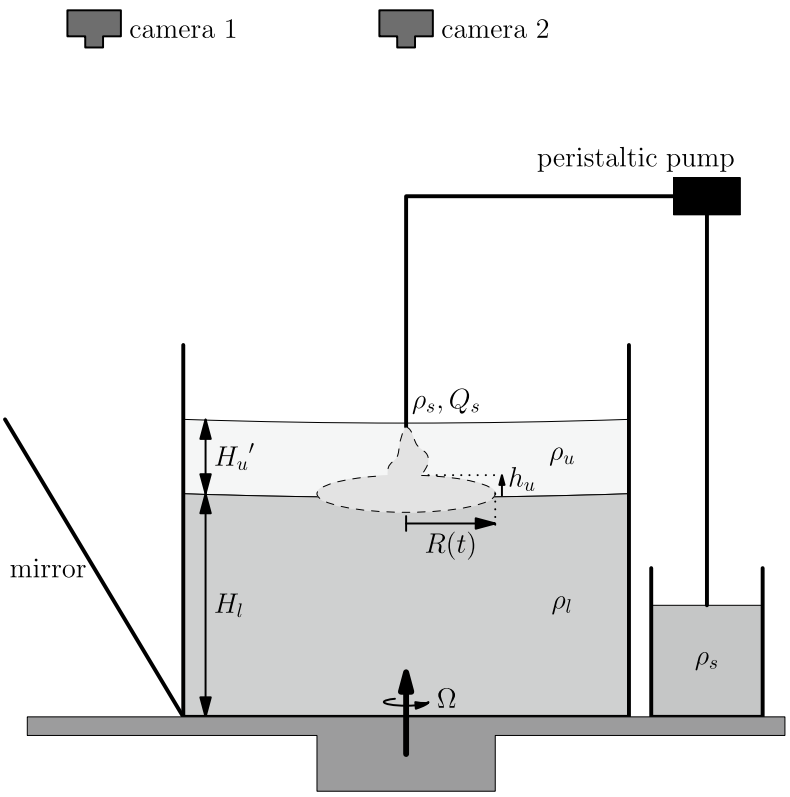

Fig. 1 Schematic of the experimental apparatus illustrating the spreading of plume fluid at the interface before penetration occurs. A tank of a square horizontal cross-section, 50 cm × 50 cm, and depth of 50 cm is placed on a turntable which rotates at angular frequency Ω. The salt water in the lower layer has density ρ_l and thickness H_l; the upper layer is filled with fresh water of density ρ_u. The respective vertical distances from the nozzle and virtual source to the interface are H_u' and H_u. Saline water of density $\rho_s > \rho_l$ flows through the nozzle with a volume flux Q_s. Camera 1 is used to record the side view movie through the angled mirror and camera 2 is used for top view recording

2.1 Plume theory

2.1.1 Non-rotating plumes

At early times the influence of background rotation on the plume is insignificant, thus the properties of the plume can be estimated from the MTT model [21]. In a uniform density ambient fluid without rotation, the reduced gravity, $g'(z)$, vertical velocity, $w(z)$, and radius, $b(z)$, of a top-hat plume are given by the MTT equations [21]:

$$g'(z) = \frac{5}{6\alpha}\left(\frac{10}{9\alpha}\right)^{\frac{1}{3}}\pi^{-\frac{2}{3}}F_s^{2/3}z^{-5/3}, \tag{1}$$

$$w(z) = \frac{5}{6\alpha}\left(\frac{9\alpha}{10}\right)^{\frac{1}{3}}\pi^{-\frac{1}{3}}F_s^{1/3}z^{-1/3}, \tag{2}$$

$$b(z) = \frac{6}{5}\alpha z. \tag{3}$$

Here z is the vertical distance from the ideal plume source with the positive direction downwards, $g' = g(\rho(z) - \rho_u)/\rho_u$ is the reduced gravity of the plume with respect to the upper layer ambient fluid of density ρ_u, g is gravity, F_s is the source buoyancy flux and α is the entrainment coefficient. A typical value of α for a top-hat plume is 0.14, through different studies have reported values as low as 0.1 and as high as 0.16 [6].

If a (descending) plume impinges upon a density interface in two-layer fluid situated a distance H_u below the virtual origin, whether or not it penetrates through the density interface depends upon the local plume density relative to the lower layer density. In this context, it is helpful to introduce the buoyancy parameter employed by Mott and Woods [22] and Ma et al. [20]

$$\Lambda = \frac{g'(H_u)}{g'_{ul}} \simeq 5.5\frac{{F_s}^{2/3}}{{H_u}^{5/3} g'_{ul}}. \tag{4}$$

Here $g'_{ul} = g(\rho_l - \rho_u)/\rho_u$ is the reduced gravity of the lower layer of density ρ_l with respect to the upper layer of density ρ_u. In (4) Λ characterizes the initial and source conditions under the assumption that the plume is negligibly affected by rotation when first reaching the density interface.

2.1.2 Effects of background rotation on the plume

Although Λ may prove a helpful metric at early times, the later evolution of the plume will be affected by the background rotation rendering invalid the entrainment and self-similarity assumptions adopted by MTT. In principle, the Coriolis force can reduce the volume of fluid entrained into a plume by suppressing the horizontal motion of turbulent eddies. At depth z, the local characteristic length and velocity scales of the largest eddy within a plume are given by the radius, $b(z)$, and the mean vertical velocity, $w(z)$, respectively. The relative importance of the Coriolis force on an eddy of this size and speed is assessed by a depth-dependent Rossby number defined as

$$\mathrm{Ro}\,(z) = \frac{w(z)}{fb(z)}, \tag{5}$$

where $f = 2\Omega$ is the Coriolis parameter. Substituting (2) and (3) into (5), yields

$$\mathrm{Ro}\,(z) = \frac{25}{72}\left(\frac{9}{10\pi\alpha^5}\right)^{1/3} \Omega^{-1} F_s^{1/3} z^{-4/3} \approx 6.0\frac{F_s^{1/3}}{\Omega z^{4/3}}, \tag{6}$$

which confirms that rotation becomes more important with distance from the source. In particular, Fernando et al. [10] found that the radius of a plume ceased to increase with depth after reaching a critical depth $z_c \simeq (3.3 \pm 0.3)(F_s/\Omega^3)^{1/4}$. Putting this into (6) gives the corresponding Rossby number at this depth to be approximately $\mathrm{Ro}_c \simeq 1.2$. Thus, at least during its initial evolution, rotation has negligible influence upon the plume at depths z where $\mathrm{Ro}\,(z) \gg \mathrm{Ro}_c$.

For a plume in a two-layer fluid with vertical distance H_u between the ideal source and the density interface, rotation should have negligible influence on the eddies if

Ro $(H_u) \gg 1$. On the other hand, because the radial horizontal flow into the plume is smaller than w by almost an order of magnitude, the Coriolis force can alter the direction of this flow such that a cyclonic circulation forms around the plume. Such a circulation will inhibit further entrainment but may become unstable in time [10] according to which the amount of fluid entrained into the plume could vary as a function of t. A further consideration is that plumes may precess as a consequence of background rotation. Such a precession, which is due to the adverse vertical pressure gradient set up by Coriolis forces [28], is potentially significant: the plume trajectory is then angled rather than vertically-downwards. Accordingly, there is a greater distance over which ambient fluid may be entrained into the plume core. These dynamics suggest that the plume entrainment coefficient, α, likely changes in the presence of background rotation. Although this dependence is likely to be progressive so that larger Ω results in larger values of α, the precise variation of the entrainment coefficient with Ro has not yet been explored quantitatively through either laboratory experiments or numerical simulations.

We reiterate, therefore, that Λ characterizes the initial and source conditions but is not necessarily representative of the relative density of the plume at the interface for large time, t. Despite this, it will be shown that measurements of the penetration time, normalized by Ω, show good collapse with Λ. We thereby draw an important and non-intuitive link between the rotating and non-rotating cases, characterized as they are by significantly different dynamical processes.

2.2 Advance of non-rotating and rotating intrusions

Under the shallow-water approximation for incompressible and Boussinesq flow in a non-rotating, uniform ambient density fluid, the radial advance of an axisymmetric gravity current driven by a constant buoyancy flux, F_s, at the source is given by

$$R(t) \propto \left(F_s t^3\right)^{1/4}, \tag{7}$$

where the proportionality constant was measured from experiments to be 0.84 ± 0.06 [4]. Extensions to Britter's [4] analysis have considered (dense) axisymmetric gravity currents fed not by a floor-level source but rather by a descending thermal [25] or plume [17]. In the latter case, Kaye and Hunt [17] modelled the radial outflow due to plume impingement on the rigid bottom boundary as jet-like near the site of impingement and gravity current-like in the far-field, taken to be at distances greater than 4.3 times the plume radius at the point of impingement. Beyond this radius, they obtained the same semi-empirical prediction as Britter [4]. In our experiments of plume impingement upon a density interface, the plume initially overshoots the interface forming a fountain head. This acts to buffer the deflection of momentum from vertical to radial, but also allows for entrainment of lower layer fluid into the fountain head thus potentially changing the buoyancy flux associated with the (intrusive) gravity current.

Even if the ambient fluid initially is in solid body rotation, it is anticipated that the initial spread of the gravity current should not be influenced by rotation at early times before the flow feels background rotation. Later, Coriolis forces act to deflect the radially spreading current such that it develops into an anticyclonic lens. In the simple case considered by Griffiths and Linden [13], a constant volume flux of buoyant fluid filled a radially expanding and deepening lens. When the lens was not too deep compared with the ambient depth

they, in effect, approximated the shape of the quasi-geostrophically balanced lens as a paraboloid and so estimated the radius to increase according to

$$R(t) \propto \left(F_s t/\Omega^2\right)^{1/4} \tag{8}$$

with the maximum thickness of the lens increasing according to $h(t) \propto \Omega\left(F_s t\right)^{1/2}/g_s'$, where g_s' is the reduced gravity of the source fluid relative to the ambient fluid. Hence the lens aspect ratio, h / R, was predicted to increase as $t^{1/4}$. Helfrich and Battisti [14] and Bush and Woods [5] studied the evolution of a plume in a rotating uniformly stratified fluid. They found that the expanding lens, being fed by the plume spreading at its neutral buoyancy level, had a constant aspect ratio being set by the ratio of the Coriolis frequency to the buoyancy frequency. Thus the radius was estimated to increase according to [30]

$$R(t) \propto \left(Q_{\text{in}} Nt/\Omega\right)^{1/3}, \tag{9}$$

in which Q_{in} is a constant volume flux of fluid discharged into the intrusion.

The dynamics occurring in our experiments are qualitatively different from Griffiths and Linden [13], Helfrich and Battisti [14] and Bush and Woods [5]. Nonetheless, we expect that Coriolis forces should inhibit the radial advance of the intrusion at late times and hence that the power law exponent for R as a function of t should be higher at early times and smaller at later times.

3 Experimental setup

The experimental setup is shown in Fig. 1 and the parameters for the experiments analyzed here are listed in Table 1. All experiments were performed on a 1 m diameter turntable (ANUTECH) that provided a constant rotation at angular frequencies, Ω, ranging from 0.05 to 0.6 s^{-1} with an accuracy of 0.001 s^{-1}. An acrylic cubical tank having a horizontal cross section of 50 cm × 50 cm and depth of 50 cm was used for the experiments examining both the radial spread of the intrusion and lens as well as the penetration of the plume. Another tank having a cylindrical geometry with a diameter of 90 cm and depth of 30 cm was used for experiments examining the radial advance of the intrusion and lens over larger horizontal distances. Experiments in this tank, in comparison with the cubical tank experiments, also served to examine the influence of side walls upon the radial flows. In particular, two experiments (numbered 27 and 28 in Table 1) with the same parameters were performed in both the cubical and cylindrical tanks. At $t = 280$ s the diameters of the interfacial intrusions were measured to be 37.6 cm (cubical tank) and 40.9 cm (cylindrical tank). The relative difference being less than 8% provides evidence that the interfacial intrusion is negligibly influenced by sidewall effects if the diameter of the intrusion is less than 75% of the length/diameter of the tank. To this end, values for Ω were chosen predominantly so that plume penetration occurred before the radial flows interacted with the tank sidewalls. As documented in Table 1, such sidewall interactions occurred only in three cases (Experiments 9, 25 and 27). In this capacity and as noted above, our experiments were fundamentally different in their design vs. those of Kumagai [18] and Mott and Woods [22] for whom $\Omega = 0$ and the presence of the sidewall was therefore essential in establishing the filling-box-type flow that led to a gradual increase in the density of the fluid discharged by the plume.

Table 1 Experiment parameters

Expt.	Ω (rad s^{-1})	ρ_l (g cm^{-3})	ρ_s (g cm^{-3})	Q_s (cm^3 s^{-1})	H_u (cm)	Λ	Ro (H_u)	T_p (s)
1	0.05	1.0076	1.0705	0.87	4.6	0.83	61.5	60
2	0.05	1.0078	1.0706	0.94	5.6	0.62	49.2	118
3	0.1	1.0075	1.0700	0.94	4.5	0.93	32.9	33
4	0.1	1.0078	1.0692	0.89	5.4	0.61	24.7	99
5	0.1	1.0078	1.0704	0.92	5.4	0.63	25.1	75
6	0.1	1.0077	1.0686	0.92	6.4	0.46	19.8	108
7	0.1	1.0077	1.0688	0.91	7.4	0.36	16.3	237
8	0.1	1.0195	1.0720	0.88	4.7	0.35	30.2	160
9	0.1	1.0077	1.0695	0.98	8.2	0.30	14.8	> 240
10	0.1	1.0768	1.0715	0.95	5.5	0.07	25.3	NSV
11	0.2	1.0079	1.0706	0.81	4.4	0.84	16.1	37
12	0.2	1.0075	1.0665	0.97	5.5	0.64	12.4	54
13	0.2	1.0078	1.0667	1.02	6.5	0.48	10.0	77
14	0.2	1.0079	1.0693	0.95	7.5	0.36	8.3	232
15	0.2	1.0080	1.0678	0.60	7.0	0.27	9.1	U
16	0.3	1.0077	1.0704	0.87	4.5	0.85	10.6	20
17	0.3	1.0078	1.0692	0.90	5.4	0.62	8.3	39
18	0.3	1.0078	1.0691	0.91	6.4	0.46	6.6	90
19	0.3	1.0079	1.0671	1.10	7.6	0.39	5.6	133
20	0.3	1.0078	1.0667	0.96	7.5	0.36	5.4	192
21	0.3	1.0078	1.0678	0.65	7.0	0.29	6.0	U
22	0.3	1.0207	1.0720	0.98	5.5	0.28	8.5	190
23	0.3	1.0243	1.0711	0.93	5.4	0.21	8.4	NSV
24	0.3	1.0288	1.0710	0.67	5.3	0.15	7.9	NSV
25	0.3	1.0752	1.1370	0.85	5.2	0.11	10.7	> 840
26	0.3	1.0538	1.0718	0.99	5.5	0.10	8.5	NSV
27	0.3	1.0750	1.0705	1.02	5.5	0.07	8.5	> 480
28	0.3	1.0760	1.0712	0.98	5.5	0.07	8.5	NSV
29	0.3	1.0735	1.0530	1.10	11.7	0.02	2.9	NSV
30	0.4	1.0079	1.0697	0.90	4.5	0.84	7.9	18
31	0.4	1.0077	1.0697	0.89	5.4	0.62	6.2	26
32	0.4	1.0079	1.0670	1.02	6.5	0.47	5.0	58
33	0.4	1.0079	1.0694	1.04	7.5	0.38	4.2	112
34	0.4	1.0077	1.0689	0.93	8.5	0.29	3.5	233
35	0.4	1.0078	1.0669	0.10	5.6	0.12	6.1	U
36	0.5	1.0078	1.0694	0.84	5.4	0.59	4.9	28
37	0.5	1.0077	1.0696	0.91	6.4	0.46	4.0	49
38	0.5	1.0174	1.0721	1.01	4.9	0.37	5.9	85
39	0.5	1.0077	1.0696	0.88	7.4	0.36	3.3	81
40	0.5	1.0079	1.0695	0.90	7.4	0.36	3.3	87
41	0.5	1.0078	1.0701	0.93	8.5	0.30	2.8	157
42	0.5	1.0199	1.0719	0.88	5.2	0.29	5.3	116
43	0.5	1.0080	1.0687	0.95	8.5	0.29	2.8	131
44	0.5	1.0077	1.0703	0.93	9.4	0.25	2.4	308

Table 1 (continued)

Expt.	Ω (rad s^{-1})	ρ_l (g cm^{-3})	ρ_s (g cm^{-3})	Q_s (cm^3 s^{-1})	H_u (cm)	Λ	Ro (H_u)	T_p (s)
45	0.5	1.0754	1.0707	0.92	5.4	0.07	5.0	U
46	0.6	1.0768	1.0715	0.84	5.4	0.07	4.1	NSV

Experiment numbers are given in bold font for experiments performed in the cylindrical tank. The remaining experiments were performed in the cubical tank. The upper layer fluid density, ρ_u, is 0.9985 g cm^{-3} for all experiments

Variables are defined as Ω: angular frequency; ρ_l: lower layer density; ρ_s: plume source density; Q_s: plume source volume flux; H_u: effective upper layer thickness; Λ: buoyancy parameter defined by (4); Ro (H_u): plume interfacial Rossby number; T_p: penetration time

In some experiments penetration was not observed because there was no side-view (NSV) for the cylindrical tank experiments, because the quasigeostrophic lens became unstable (U) or because no penetration occurred before the lens expanded to the tank sidewalls (this time being indicated for Experiments 9, 25 and 27)

Prior to the initiation of rotation, the tank was filled to a depth of $H_l = 25.0$ cm with saline water having a density of ρ_l. Values for ρ_l fell into one of two categories: either 1.0075 g cm^{-3} $\leqslant \rho_l \leqslant$ 1.0080 g cm^{-3} or 1.0174 g cm^{-3} $\leqslant \rho_l \leqslant$ 1.0207 g cm^{-3}. Densities were measured at a reference temperature of 20°C with a densitometer (Anton Paar DMA 4500) having a precision of $\pm$0.00001 g cm^{-3}. Experiments were performed in a laboratory having a room temperature that fluctuated between 22°C and 23°C, which resulted in measurement uncertainties of 0.0002 g cm^{-3}.

A plume nozzle (designed by Dr. Paul Cooper and described in more detail by Hunt and Linden [16]) was suspended vertically above the lower layer along the axis of the rotation. The nozzle had a circular opening whose diameter measured 0.4 cm. Although the source volume flux, Q_s, was relatively small (i.e. 1.00 cm^3 s^{-1} in a typical experiment), the plume was observed to become turbulent close to the source, a transition aided by the addition of a small piece of fluctuation-inducing mesh to the nozzle opening. The vertical distance between the nozzle opening and the lower layer free surface was defined as the upper layer thickness H'_u where 3.0 cm $\leq H'_u \leq$ 8.0 cm. The effective upper layer thickness is taken to be $H_u = H'_u + z_v$, in which z_v is the virtual origin; z_v accounts for the fact that the nozzle has a finite area and the plume has a finite source volume flux, Q_s [15]. Together with Ω and Q_s, the range of H'_u was chosen so that in all experiments the Rossby number of the plume given by (6) evaluated at $z = H_u$ was larger than the critical Rossby number of Ro$_c \simeq 1.2$ [10].

The tank was then put into solid-body rotation allowing 30 min to elapse after the initiation of rotation. An upper layer of density $\rho_u = 0.9985$ g cm^{-3} was then added through a sponge float over top of the lower layer until the free surface was approximately 0.5 cm above the nozzle opening. Any air bubbles at the nozzle source were manually removed.

The system rotated for another hour to ensure a state of solid-body rotation throughout the entire depth of the ambient fluid. The maximum parabolic deflection of the free surface and the density interface [27] were estimated to be less than 0.2 cm for the fastest rotation rate examined ($\Omega = 0.6$ s^{-1}). In most experiments, the deflection of the interface is much less than the upper layer thickness (itself being much less than the radius of the domain). Therefore it was assumed the deflection had negligible influence upon the intrusion propagation.

The plume was generated using a peristaltic pump (Manostat Carter) to force saline water of density 1.0669 g cm $^{-3} \leqslant \rho_s \leqslant$ 1.0721 g cm $^{-3}$ through the nozzle at a volume flux Q_s ranging from 0.1 to 1.1 cm ^{3} s $^{-1}$. This fluid was drawn from a 8 L source reservoir, which was located just beneath the tank and which rotated with the same angular frequency. Before the start of each experiment the volume flux was calibrated by measuring the volume of fluid discharged by the nozzle into a graduated cylinder over a time interval of 150 s.

Two cameras secured to the frame of the rotating table were used to record experimental movies. Side-view movies were obtained with a digital camera set in movie mode (Canon EOS REBEL T2i), which was directed downwards to an angled flat mirror so that light reaching the camera passed parallel to the density interface. Lighting for the side view movies was provided by a light stand comprised of four horizontally stacked fluorescent bulbs, which was situated opposite to the angled mirror. A piece of translucent mylar paper was fastened to the tank wall adjacent to the fluorescent bulbs to diffuse the intense light produced by these bulbs. Side view movies were collected only when using the cubical tank; with the (larger) cylindrical tank, unacceptable optical distortions were present owing to the curved boundary. Top view movies were obtained with a digital movie camera (Panasonic HDC-HS250) directed downwards along the axis of rotation at a vertical distance of 2 m above the base of the tank. Here, illumination was provided using an electroluminescent light sheet placed under the tank.

After each experiment the movies were loaded into Matlab for further analysis, as described in the next section. Of the several experiments that were performed, the parameters for 46 of these are listed in Table 1. Not listed are a small number of non-rotating experiments that were performed for comparison with some corresponding rotating cases. The comparison is briefly highlighted in Sect. 5.

4 Experimental analyses and results

4.1 Analysis methods and qualitative results

An experiment begins once the peristaltic pump supplies fluid to the nozzle and a descending plume is formed. The point in time when the plume first reaches the density interface is regarded as $t = 0$. Figure 2 shows the general features from a typical experiment; here $\Omega = 0.2$ s $^{-1}$, $\rho_l = 1.0078$ g cm $^{-3}$, $\rho_s = 1.0667$ g cm $^{-3}$, $Q_s = 1.02$ cm ^{3} s $^{-1}$, and $H'_u = 5.3$ cm. The virtual origin for this experiment is calculated to be $z_v = 0.96$ cm [15]. Accordingly, we define the effective upper layer thickness as $H_u = H'_u + z_v = 6.3$ cm with the origin of the coordinate system coincident with the virtual source. Even though $\rho_s > \rho_l$, the density of the plume, ρ, decreases during its descent through the upper layer due to entrainment of upper layer fluid, so that $\rho(H_u) < \rho_l$ and hence discharged plume fluid accumulates along the interface. More specifically, this discharged fluid forms a radially spreading interfacial gravity current that in turn evolves into an anticyclonically rotating lens having a relatively slow rate of expansion (see Fig. 2a). Throughout this process, and consistent with Ezhova et al. [8, 9], ambient interfacial waves, whose influence is omitted in Sect. 2.2, were not clearly observed. As time progresses the plume entrains the relatively more dense fluid in the lens until its density at the interface exceeds that of the lower layer. Thereafter the fluid from the plume reaching the interface no longer rebounds at the fountain head, but

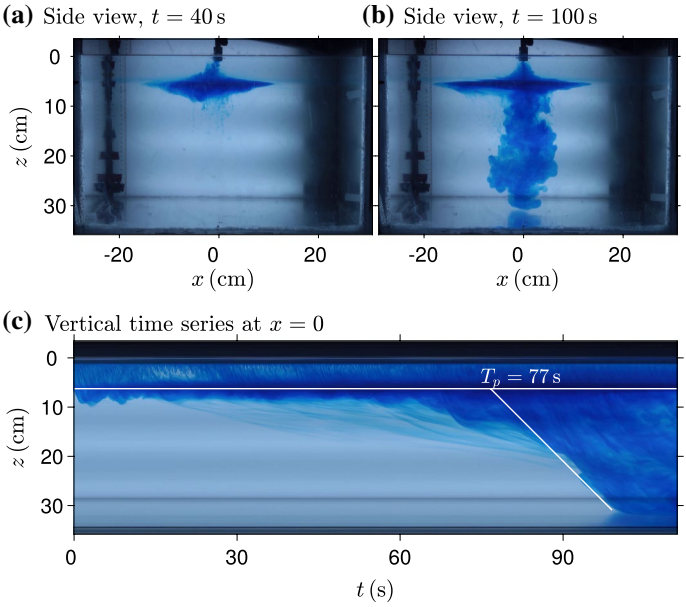

Fig. 2 Two snapshots from the side view movie of Experiment 13 (see Table 1) for which $\Omega = 0.2$ rad s^{-1} and $H_u = 6.5$ cm showing **a** at $t = 40$ s the discharged plume fluid spreads radially at the interface, **b** at $t = 100$ s when fluid has penetrated through the density interface, and **c** a vertical time series constructed below the location of the nozzle, at $x = 0$. The interface level, $z = 6.3$ cm is marked with the horizontal white line. The evolution of the plume that descends into the lower layer is determined by fitting a contour-matching straight line over the height range 15 cm $\leq z \leq$ 30 cm. The onset of penetration, $T_p = 77$ s, is estimated from the intersection point between the sloping and horizontal white lines. The bulge below the interface from 65 to 90 s indicates an accelerated thickening of the lower portion of the lens. Though often a precursor to penetration, we regard this thickening as still separate from the penetrative process

instead descends to the bottom of the tank (Fig. 2b). A vertical time series was constructed from slices through successive frames of the side-view camera movie and taken below the nozzle. This is used to estimate the time, T_p, when penetration through the interface first occurs (Fig. 2c). This is found by fitting a line to the descending front of the plume in the lower layer and extrapolating back to the level of the density interface. Fitting using a straight line is justified here because we find that, immediately post-penetration, discharged plume fluid falls at a nearly constant speed to the bottom of the tank. This is indicated by the inclined solid line in Fig. 2c. For the experiment illustrated in Fig. 2, we estimate a penetration time of $T_p = 77$ s; data corresponding to other experiments, including those for which penetration was not observed, are summarized in Table 1 and are discussed further below.

In most experiments, the plume near the source begins to precess a short time after the start of the experiment (Frank et al. [12] observed this to occur between one-half and one background rotation periods). Figure 3a, b show zoomed-in snapshots focusing on the region around the nozzle from the same experiment shown in Fig. 2, for which $\Omega = 0.2$ rad s^{-1}. The plume deflects to the right at $t = 20$ s and to the left at $t = 40$ s. To make this oscillatory behaviour more evident, horizontal time series are constructed from the experimental movie at $z = 3.5$ cm as shown in Fig. 3c. The precession period is measured to be approximately 40 s in this particular case, corresponding to a precession

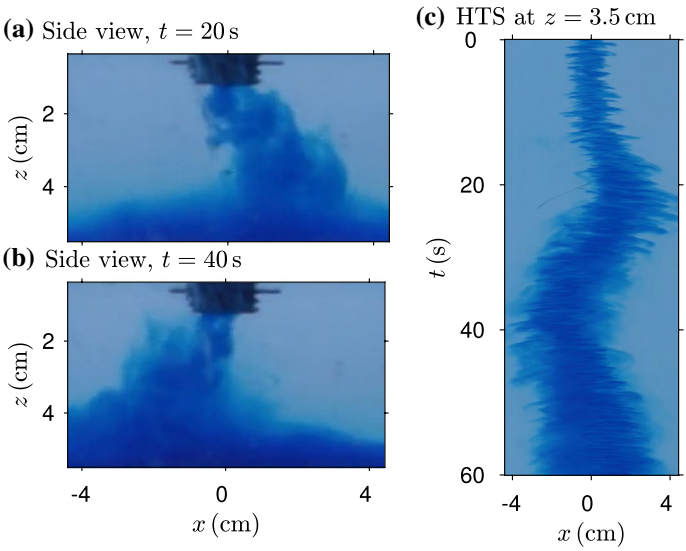

Fig. 3 Zoomed-in snapshots of the region close to the nozzle from the side view movie of the experiment shown in Fig. 2. The plume is declined to the right at **a** $t = 20$ s, and to the left at **b** $t = 40$ s. A horizontal time series (HTS) constructed from the movie at $z = 3.5$ cm is shown in panel (**c**)

frequency of 0.16 s^{-1}. Also evident in Fig. 3c is the gradual thickening of the plume in time at this fixed depth below the source. This is due to the encroachment from below of the thickening lens and the opposing vertical pressure gradient forces set up by rotation that are responsible for the precession of the plume [12, 28].

In spite of the precession described above, it is clear from Fig. 2a, b that the lens of Experiment 13 remained below the plume up to and beyond the onset of plume penetration into the lower layer. However in a smaller number of experiments (4 of 46), the lens shifted its position off centre and/or broke into a pair of smaller vortices. Such behaviour is noted, for instance, in Fig. 4, which presents snapshots from both-side and top-view movies for Experiment 21. At early times, this experiment is similar to that shown in Fig. 2a before penetration: discharged plume fluid collected below the nozzle and rotated anticyclonically. However, before the plume was able to penetrate through the density interface, the lens became non-axisymmetric. In a similar case of a plume descending in a rotating uniform fluid, Fernando et al. [10] also found an instability of the outflow formed by the plume fluid impinging upon the bottom—see e.g. their figure 5. Fernando et al. [10] attributed this instability to a baroclinic instability. (Similar conclusions were drawn by Griffiths and Linden [13] who also observed that their free surface lenses became unstable in the long time limit.) Whereas this instability was quite prevalent in Fernando et al.'s study where discharged plume fluid had no alternative but to accumulate along the lower (impermeable) boundary, our experiments are qualitatively different: penetration of discharged plume fluid into the lower layer typically occurred well before the onset of the baroclinic instability. In other words, we only rarely observed the non-axisymmetric flow structures exhibited in Fig. 4. When these appeared and the lens shifted off-centre, the plume fluid then passed through only a thin part of the lens and so penetration into the lower layer was not observed in a duration of 310 s, whereas in comparable experiments with no instability, penetration was observed within this time.

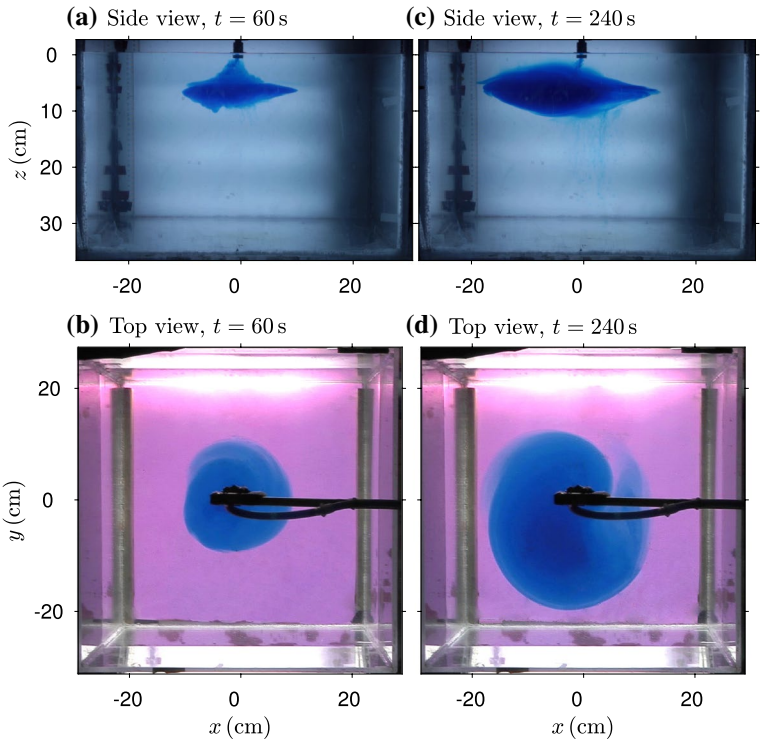

Fig. 4 Snapshots from both side view and top view movies of Experiment 21 (Table 1). The other horizontal axis in the top view images is indicated as y with origin located at the nozzle. Here, an instability causes the lens to become non-axisymmetric and move off-centre between $t = 60$ s and $t = 240$ s. Consequently, no penetration is observed. A metal rod is used to suspend the nozzle above the tank; it appears, (along with the tubing supplying the nozzle) as a horizontal line in panels **b** and **d**

In some other experiments (not listed in Table 1), the time to penetration, T_p, was substantially reduced because the plume developed into a tubular cyclonic vortex, which penetrated from the upper to the lower ambient fluid. Consistent with uniform ambient experiments conducted by Dr. Daria Frank at U. Cambridge where a similar kind of vortex appeared (personal communication), the evolution of the plume was rendered dramatically different in these cases but, unfortunately, it proved very difficult to reproduce the tubular cyclonic vortex even in experiments with ostensibly identical initial/source conditions. Because of this fact, we defer further discussion of this vortex to future studies, experiments and numerical simulations for which are presently underway.

Whether or not there appears a baroclinic instability of the type described above, it is possible to infer an intrusion radius from top view images such as those exhibited in Fig. 4b. For each frame from the top view movie, the plan area, $S(t)$, of the intrusion is calculated, from which the effective radius of the intrusion is obtained to be $R^*(t) = \sqrt{S(t)/\pi}$, where $*$ indicates a value obtained by experimental measurement.

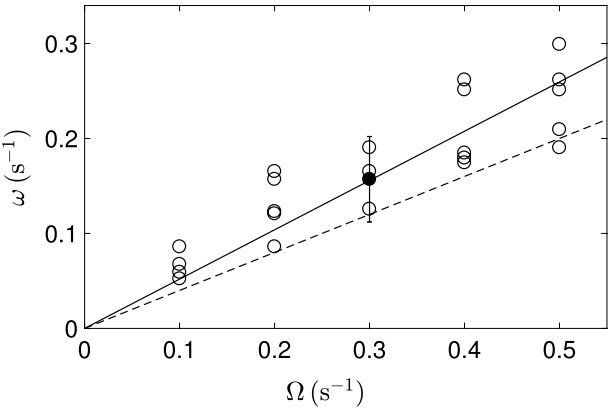

Fig. 5 Frequency of plume precession, ω, plotted against the background rotation rate, Ω. A representative error bar is plotted on the closed symbol. The best-fit line is indicated as the solid line and the dashed line shows the result of Frank et al. [12]

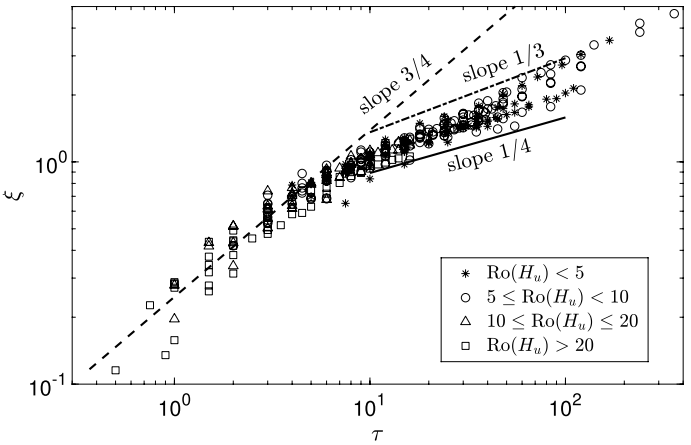

Fig. 6 Non-dimensional radial position of the intrusion front, ξ, versus non-dimensional time, τ. The best-fit line with a slope of 3 / 4 for $\tau < 5$ is given by the dashed line. The solid and dash-dotted lines indicate the straight lines with slopes of 1 / 4 and 1 / 3, respectively

4.2 Quantitative results

Figure 5 shows a plot of the frequency of precession, ω, versus the background rotation frequency Ω. In their study of plumes in a rotating uniform density ambient fluid, Frank et al. [12] found that ω increased linearly with Ω with a proportionality constant of 0.40 ± 0.04. Likewise we find an approximately linear relationship between ω and Ω, although with a moderately larger ratio of 0.52 ± 0.09. The reasons for this discrepancy are unknown but may be influenced by the presence of the anticyclonic lens, which was absent in Frank et al.'s study.

In examining the radial advance of the early-time interfacial gravity current and the late-time lens, we nondimensionalize time by $\tau \equiv \Omega t$ and, motivated by the gravity current prediction (7), we nondimensionalize the radial position by $\xi \equiv R^*/(F_s/\Omega^3)^{1/4}$. Figure 6 shows the corresponding plot of ξ versus τ. As anticipated, we find a rapid increase in

radius at early times followed by a slower advance at later times. Our data at small τ span more than an order of magnitude in Λ, i.e. $0.07 \leq \Lambda \leq 0.9$. Notwithstanding some scatter, the data collapse reasonably well suggesting that the relationship between ξ and τ is insignificantly influenced by Λ in the intrusive gravity current spreading regime. For $\tau < 5$, we fit the measured data in Fig. 6 with a straight line for each individual experiment. The slopes, p_i, of these best-fit lines are plotted versus Λ in Fig. 7. The values of p_i fluctuate by about 50% around the value of 3/4, which is the power law exponent predicted for an intrusive axisymmetric gravity current [4, 17]. Forcing a best-fit line through all the data for $\tau < 5$ to have a 3/4 slope we compute the intercept thus giving the empirical estimate for the radius as a function of time at early times:

$$R(t) = [0.25 \pm 0.05]\left(F_s t^3\right)^{1/4}, \quad \text{for } \tau < 5. \tag{10}$$

At large times, the non-dimensional radius, ξ, shows a wider and generally more systematic range of power law behaviours. For $\tau > 10$, we again fit the data points from each individual experiment in Fig. 6 with a straight line; the resulting slopes, p_l, are also shown in Fig. 7. (Note that for most experiments it was not possible to measure the radius both of the intrusion at early times ($\tau \lesssim 5$) and the lens at late times ($\tau \gtrsim 10$) either because fast rotation resulted in rapid development of the lens or slow rotation meant that the plume penetrated or, in more select instances, the intrusion reached the side walls of the tank before rotation became significant.) For experiments with $\Lambda \gtrsim 0.2$, the values of p_l fluctuate around 1/4, the same value derived by [13] in their experiments of a lens fed by a point source (not a plume) and expanding just below a free surface. For experiments with $\Lambda \lesssim 0.2$, p_l holds values around 0.42 in all but one experiment (Experiment 10), which featured not only a small value for $\Lambda \simeq 0.07$, but also a low rotation rate of $\Omega = 0.1$ rad s^{-1}. Generally, it is anticipated that the power law is set not only by Λ but also by Ro; theoretically confirming this fact remains an open problem to be pursued in future investigations.

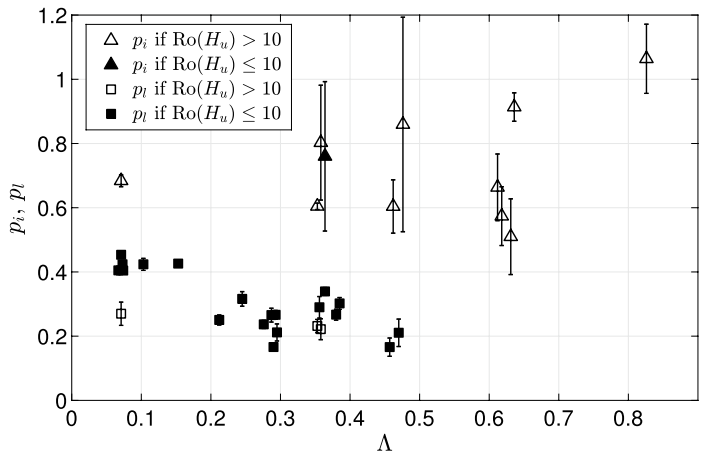

Fig. 7 The slopes, p_i for $\tau < 5$ and p_l for $\tau > 10$, of the best-fit lines of the data points from each individual experiment in Fig. 6. The open and closed symbols represent experiments with large and small Ro(H_u), respectively

It takes more time for the plume to increase its density at the interface to the point of penetration if the initial density of the plume at the interface is much less than the density of the lower layer. Symbolically, we expect T_p to increase as Λ decreases. Also the lens radius is expected to increase at a slower rate with increasing Ω, so that the thickness of the lens is expected to increase at a faster rate. Thus the plume re-entrains the comparatively larger density fluid of the lens over a greater depth making its density at the interface larger, suggesting that T_p decreases as Ω increases.

Corroborating the above reasoning, the non-dimensional penetration time $\tau_p = \Omega T_p$ is plotted against Λ in Fig. 8. Excluded from this data set are experiments where penetration was not observed within the duration of the experiment whether because of baroclinic instability or because the lens extended to the sidewalls before penetration occurred. Overwhelmingly, such cases are associated with small values of Λ where, as just noted, we expect the onset of penetration to be significantly delayed. Indeed, Table 1 indicates that penetration was avoided only three times when $\Lambda \geq 0.21$ (i.e. in Experiments 9, 15 and 21) and in two of these experiments (i.e. Experiments 15 and 21), there appeared a baroclinic instability of the type exhibited in Fig. 4. The measured data of Fig. 8 collapse well suggesting that the penetration time has a simple relationship with Ω and Λ. This relationship can be inferred from the inset to Fig. 8, which shows $\log_{10}(\tau_p)$ vs. $\log_{10}(\Lambda)$ and which also includes a line of best fit, i.e.

$$\tau_p \equiv T_p \Omega = (2.7 \pm 0.5)\Lambda^{-2.7\pm0.2}. \tag{11}$$

In comparison, the characteristic time-scale employed by [22] to normalize the penetration time from their non-rotating experiments was a buoyancy time, which was a function of the horizontal cross-sectional area of the tank. In our rotating experiments the lens almost never reaches the vertical sidewalls. The tank cross-sectional area is therefore of subordinate importance and it is thus more appropriate to take $1/\Omega$ as the characteristic time in (11). Note that (11) cannot be employed in the limiting case of immediate penetration, $\Lambda \to 1$, for which $\tau_p \to 0$ is expected. In such a limiting case, no horizontal spreading occurs at the density interface and thus the above discussed processes of lens re-entrainment into the plume and fountain-head entrainment do not occur. Thus (11) should

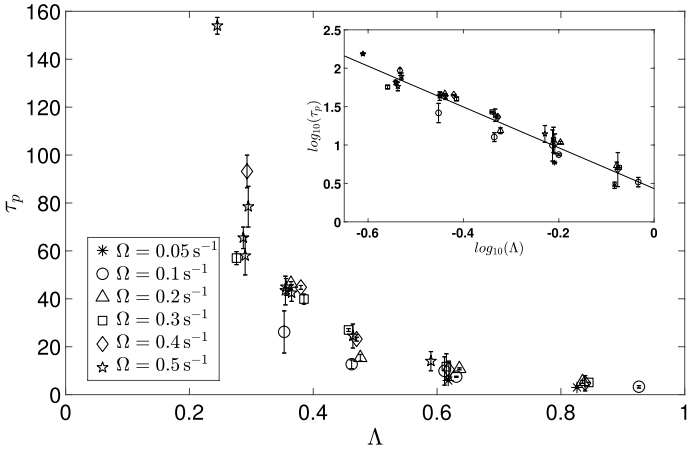

Fig. 8 Non-dimensional penetration time, τ_p, versus Λ. The inset shows $\log_{10}(\tau_p)$ vs. $\log_{10}(\Lambda)$, and the solid line is a best-fit of the measurements, which is given by $\tau_p = (2.7 \pm 0.5)\Lambda^{-2.7\pm0.2}$

be interpreted to be valid only in the cases in which a horizontal intrusion (lens) forms and subsequent processes of re-entrainment and fountain-head entrainment occur. In turn, the lens should remain directly below the plume (c.f. Fig. 2) rather than moving off-centre (c.f. Fig. 4), the latter behavior being relatively uncommon in our experiments. Notwithstanding these restrictions, it is remarkable that (11) holds as broadly as it does, i.e. up to values of $\Lambda \approx 0.9$ corresponding to τ_p as low as about 3.

5 Discussion and conclusions

We have investigated a point-source plume descending into a rotating two-layer ambient fluid. Although the fluid emanating from the source is more dense than the lower layer, turbulent entrainment causes the plume to be less dense than the lower layer when the plume impinges initially upon the interface. Symbolically, this condition is expressed as $\Lambda \equiv g'(H_u)/g'_{ul} < 1$. As such, our study is similar to those of Kumagai [18] and Mott and Woods [22] except that we include background rotation, which non-trivially changes the evolution of the flow in several ways.

As regards the plume dynamics, rotation deflects the radially-inward flows associated with entrainment into the plume resulting in a cyclonic circulation in the ambient fluid around the plume [10]. Consistent with Frank et al. [12], we likewise find that rotation causes the plume to precess anticyclonically. Rotation also modifies the outflow of discharged plume fluid along the density interface. Before this horizontal flow feels the effect of rotation at small times, the intrusion falls into the intrusive gravity current regime, with the advancing distance approximately proportional to $t^{3/4}$. At later times, the outflow is deflected to form an anticyclonic lens whose radius follows a power law relationship against time with the power law exponent being approximately 1 / 4 if $\Lambda \gtrsim 0.2$ or ranging between 0.25 and 0.45 if $\Lambda \lesssim 0.2$.

The plume entrains fluid not only from the upper and lower ambient layers, but also re-entrains fluid previously discharged into the lens. As a consequence of this behaviour, the lens density steadily increases with time up until the point where it exceeds the lower layer density. This defines the onset of penetration which is characterized by discharged plume fluid starting to continuously fall to depth. Thicker lenses which occur for larger Ω, have more voluminous plume re-entrainment and consequently smaller penetration times, T_p. This is captured by the empirical relationship (11) for T_p as it depends on rotation through Ω and the relative initial buoyancy at the interface through Λ. Of critical importance as regards (11) and its potential application to real convective geophysical processes, as in the ocean, is to realize that rotation acts to accelerate penetrative breakthrough, which in turn is important to vertical transport processes. To underscore this point, we compared Experiment 3 with an analogue non-rotating experiment (not listed in Table 1). Both experiments had effectively the same source conditions and upper layer depth so that in each case $\Lambda = 0.93$. However, in the non-rotating experiment the time required for penetration was larger by a factor of nearly eight.

Clearly buoyant convection in geophysical stratified environments is more complicated than what we have modelled experimentally. In particular, toward understanding oceanic convection, future work will examine (i) the case of a deeper upper ambient layer whereby Ro $(H_u) \lesssim 1$ and the plume is more significantly impacted by rotation (c.f. figures 2 and 4 of Fernando et al. [10]), (ii) spreading and penetration of fluid originating from a horizontally distributed, rather than a point, source of negative buoyancy, and, (iii) instances where

the ambient density stratification evolves temporarily both as a result of interactions with the descending plume and also because of basin inflows and outflows c.f. Ma et al. [20].

Acknowledgements Funding for this study was generously provided by NSERC through the Discovery Grant and RTI programs.

References

1. Ayotte BA, Fernando HJS (1994) The motion of a turbulent thermal in the presence of background rotation. J Atmos Sci 51(13):1989–1994
2. Baines PG, Sparks RSJ (2005) Dynamics of giant volcanic ash clouds from supervolcanic eruptions. Geophys Res Lett 32:L24808.
3. Baines WD, Turner JS (1969) Turbulent buoyant convection from a source in a confined region. J Fluid Mech 37:51–80
4. Britter RE (1979) The spread of a negatively buoyant plume in a calm environment. Atmos Environ 13(9):1241–1247
5. Bush J, Woods AW (1999) The generation of coherent vortices by line plumes in rotating stratified fluid. J Fluid Mech 614:15–37
6. Carazzo G, Kaminski E, Tait S (2006) The route to self-similarity in turbulent jets and plumes. J Fluid Mech 547:137–148
7. Colomer J, Zieren LD, Fernando HJS (1998) Comment on "Locaalized convection in rotating stratified fluid" by J. A. Whitehead et al. J Geophys Res 103(C6):12891–12894
8. Ezhova E, Cenedese C, Brandt L (2016) Interaction between a vertical turbulent jet and a thermocline. J Phys Oceanogr 46:3415–3437
9. Ezhova E, Cenedese C, Brandt L (2017) Dynamics of a turbulent buoyant plume in a stratified fluid. J Phys Oceanogr 47:2611–2630
10. Fernando HJS, Chen Rr, Ayotte BA (1998) Development of a point plume in the presence of background rotation. Phys Fluids 10(9):2369–2383
11. Fernando HJS, Ching CY (1993) Effects of background rotation on turbulent line plumes. J Phys Oceanogr 23:2125–2129
12. Frank D, Landel JR, Dalziel SB, Linden PF (2017) Anticyclonic precession of a plume in a rotating environment. Geophys Res Lett 44(18):9400–9407.
13. Griffiths RW, Linden PF (1981) The stability of vortices in a rotating, stratified fluid. J Fluid Mech 105:283–316
14. Helfrich KR, Battisti TM (1991) Experiments on baroclinic vortex shedding from hydrothermal plumes. J Geophys Res 96(C7):12511–12518
15. Hunt GR, Kaye NG (2001) Virtual origin correction of lazy turbulent plumes. J Fluid Mech 435:377–396
16. Hunt GR, Linden PF (2001) Steady-state flows in an enclosure ventilated by buoyancy forces assisted by wind. J Fluid Mech 426:355–386
17. Kaye NB, Hunt GR (2007) Overturning in a filling box. J Fluid Mech 576:297–323
18. Kumagai M (1984) Turbulent buoyant convection from a source in a confined two-layered region. J Fluid Mech 147:105–131
19. Lemckert C, Imberger J (1993) Axisymmetric intrusive gravity currents in linearly stratified fluids. J Hydraul Eng ASCE 119:662–679
20. Ma Y, Flynn MR, Sutherland BR (2017) Convection from a line-source into a two-layer stratified ambient fluid. J Fluid Mech 818:46–67
21. Morton BR, Taylor GI, Turner JS (1956) Turbulent gravitational convection from maintained and instantaneous sources. Proc R Soc Lond Ser A 234:1–23
22. Mott RW, Woods AW (2009) On the mixing of a confined stratified fluid by a turbulent buoyant plume. J Fluid Mech 623:149–165
23. Okada N, Ikeda M, Minobe S (2004) Numerical experiments of isolated convection under polynya. J Oceanogr 60(6):927–943
24. Richards TS, Aubourg Q, Sutherland BR (2014) Radial intrusions from turbulent plumes in uniform stratification. Phys Fluids 26(036602):1–17.
25. Rooney GG (2015) Descent and spread of negatively buoyant thermals. J Fluid Mech 780:457–479
26. Rooney GG, Devenish BJ (2014) Plume rise and spread in a linearly stratified environment. Geophys Astrophys Fluid Dyn. 108(2):168–190
27. Scase MM, Baldwin KA, Hill RJA (2017) Rotating Rayleigh–Taylor instability. Phys Rev Fluids 2:024801

28. Tomàs AF, Poje AC, Özgökmen TM, Dewar WK (2016) Effects of rotation on turbulent buoyant plumes in stratified environments. J Geophys Res 121(8):5397–5417
29. Whitehead JA, Marshall J, Hufford GE (1996) Locaalized convection in rotating stratified fluid. J Geophys Res 101(C11):25705–25721
30. Woods AW (2010) Turbulent plumes in nature. Ann Rev Fluid Mech 42:391–412